Title

Imaging Structure and Composition Homogeneity of 300 mm SiGe Virtual Substrates for Advanced CMOS Applications by Scanning X-ray Diffraction Microscopy

Journal

ACS Applied Materials & Interfaces, 7(17)

ISSN

1944-8244

Authors

Zoellner, Marvin H
Richard, Marie-Ingrid
Chahine, Gilbert A
et al.

Publication Date

2015-05-06

DOI

10.1021/am508968b

Peer reviewed

ACS APPLIED MATERIALS & INTERFACES

Research Article

www.acsami.org

Imaging Structure and Composition Homogeneity of 300 mm SiGe Virtual Substrates for Advanced CMOS Applications by Scanning X-ray Diffraction Microscopy

Marvin H. Zoellner,*[,†] Marie-Ingrid Richard,[‡,§] Gilbert A. Chahine,[‡] Peter Zaumseil,[†] Christian Reich,[†] Giovanni Capellini,[†] Francesco Montalenti,[∥] Anna Marzegalli,[∥] Ya-Hong Xie,[⊥] Tobias U. Schülli,[‡] Maik Häberlen,[#] Peter Storck,[#] and Thomas Schroeder[†,▽]

[†]IHP, Im Technologiepark 25, 15236 Frankfurt (Oder), Germany

[‡]European Synchrotron Radiation Facility, BP 220, 38043 Grenoble Cedex, France

[§]Aix-Marseille Université, CNRS, IM2NP UMR 7334, 13397 Marseille Cedex 20, France

[∥]Dipartimento di Scienza dei Materiali, Università degli Studi di Milano-Bicocca, Via R. Cozzi 55, 20126 Milano, Italy

[⊥]Department of Materials Science and Engineering, University of California at Los Angeles, Los Angeles, California 90095-1595, United States

[#]Siltronic AG, Hans-Seidel-Platz 4, 81737 München, Germany

[▽]Institute for Physics and Chemistry, Brandenburgische Technische Universität Cottbus, Konrad-Zuse-Strasse 1, 03046 Cottbus, Germany

Supporting Information

ABSTRACT: Advanced semiconductor heterostructures are at the very heart of many modern technologies, including aggressively scaled complementary metal oxide semiconductor transistors for high performance computing and laser diodes for low power solid state lighting applications. The control of structural and compositional homogeneity of these semiconductor heterostructures is the key to success to further develop these state-of-the-art technologies. In this article, we report on the lateral distribution of tilt, composition, and strain across step-graded SiGe strain relaxed buffer layers on 300 mm Si(001) wafers treated with and without chemical−mechanical polishing. By using the advanced synchrotron based scanning X-ray diffraction microscopy technique K-Map together with micro-Raman spectroscopy and Atomic Force Microscopy, we are able to establish a partial correlation between real space morphology and structural properties of the sample resolved at the micrometer scale. In particular, we demonstrate that the lattice plane bending of the commonly observed cross-hatch pattern is caused by dislocations. Our results show a strong local correlation between the strain field and composition distribution, indicating that the adatom surface diffusion during growth is driven by strain field fluctuations induced by the underlying dislocation network. Finally, it is revealed that a superficial chemical−mechanical polishing of cross-hatched surfaces does not lead to any significant change of tilt, composition, and strain variation compared to that of as-grown samples.

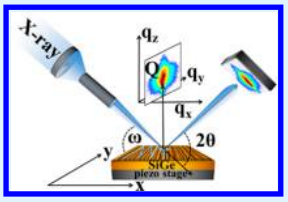

KEYWORDS: *CMOS, strain relaxed SiGe buffer, chemical−mechanical polishing, structure inhomogeneities, scanning X-ray diffraction microscopy*

1. INTRODUCTION

Advanced semiconductor heterostructures are at the very heart of many modern technologies in various application fields to address today's challenges in society. For example, high performance computing relies on aggressively scaled complementary metal oxide semiconductor (CMOS) "More Moore" technologies. The integration of alternative semiconductors on Si is an important materials science approach to improve metal oxide semiconductor field effect transistors (MOSFETs), e.g., III−V materials for n- and Ge for p-channel devices.[1,2] Furthermore, highly complex electronic−photonic integrated circuits (EPICs), e.g., wireless SiGe mixed signal radiofrequency technology with photonic sensing applications, are achieved using new materials integrated on Si following "More than Moore" approaches.[3] To address the vision of a monolithically integrated light source module in a Si CMOS environment, intense research on the integration of III−V materials as well as that on band gap engineering of group IV semiconductors is applied to achieve direct band gap materials either in the form of strained Ge or SiGeSn alloy systems.[4,5]

For these purposes, Germanium virtual substrates (VS) on large diameter Si wafers are considered as a central materials platform to enable these advanced technologies. Germanium-based VS are usually obtained by exploiting the compositional

Received: December 19, 2014
Accepted: April 14, 2015
Published: April 14, 2015

DOI: 10.1021/am508968b
ACS Appl. Mater. Interfaces 2015, 7, 9031−9037

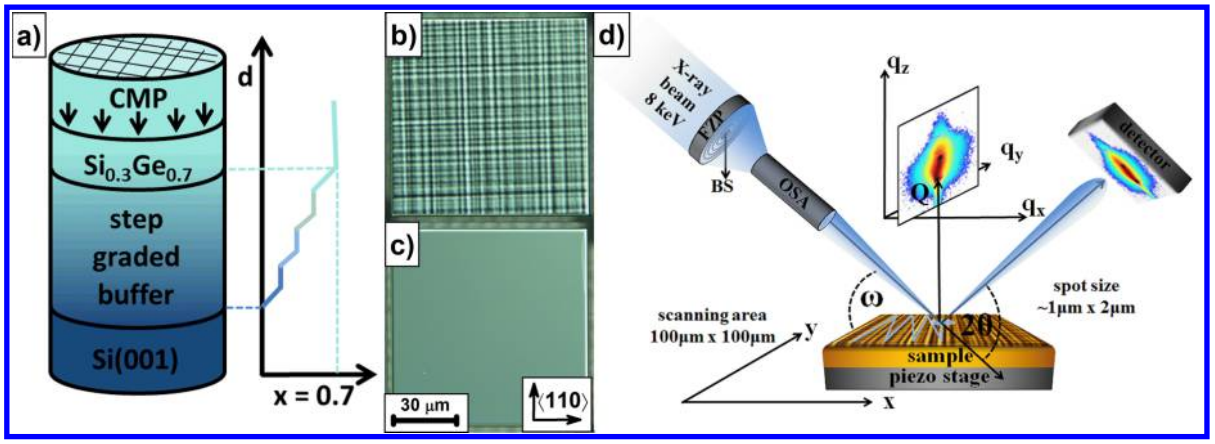

Figure 1. (a) Layer stacking of the investigated $Si_{0.3}Ge_{0.7}$ film on a step graded $Si_{1-x}Ge_x$ buffer on Si(001). Differential interference contrast images of an (b) unpolished and (c) polished sample. (d) Experimental set up of the K-Map measurements.

grading of $Si_{1-x}Ge_x$ strain-relaxed buffer (SRB) layers to reduce the misfit dislocation density by gradually lowering the lattice mismatch of the heterostructure with respect to the final functional layer.[6] For further improvements and control on defect reduction, several techniques were developed over the years, e.g., backside stressor (BSS) deposition to avoid wafer bow and microcracks,[7] annealing in combination with chemical−mechanical polishing (CMP) steps to decrease the surface roughness and reduce dislocation bunching,[8] etc. Although the overall dislocation density has been reduced to values as low as 1×10^6 cm^{-2}, inhomogeneous dislocation bunching might still lead to "dead areas" on the wafer, reducing achievable process yields. Therefore, it is of paramount importance to investigate the dislocation distribution and to understand its influence on the crystal structure and on wafer morphology. While surface undulation of lattice mismatched SiGe surfaces, the so-called *cross-hatch pattern*, has been observed for decades,[9,10] the underlying mechanism for its formation is not fully understood yet, owing to the dynamic interplay between elastic and plastic strain relaxation contributions.[11,12]

X-ray investigations, corroborated by theoretical modeling, have been shown to be of great help in characterizing buried misfit-dislocation distributions within the SiGe graded region.[13−15] Although, several other experimental techniques have been employed to determine the lateral dislocation distribution (plane-view transmission electron microscopy (TEM), electron beam-induced current (EBIC), and etch pit analysis), not so many techniques are known to simultaneously probe the local strain and composition variation on the micrometer scale, as e.g., Raman microscopy. In this work, we report on a newly developed synchrotron-based X-ray diffraction (XRD) technique, named quicK continuous mapping (K-Map).[16] K-map allows local, model-free, and nondestructive imaging of structural inhomogeneities in SiGe VS with submicrometer resolution in a fast scan mode. It is noted that, already back in 1999, Mooney et al.[17] employed an X-ray microdiffraction technique without fast scanning options to investigate local lattice tilt variations of SiGe buffer systems grown on Si(001). Similar investigations were done later on by Mochizuki et al.[18] who were able to resolve, upon using a micrometer sized X-ray beam, distinct materials inhomogeneities of SiGe crystal domains which were not observable in conventional XRD studies due to averaging effects. Recently, Mondiali et al.[19] reported K-Map measurements of $Si_{0.8}Ge_{0.2}$ films on patterned wafers. In particular, they reported intensity maps of the (004) and (113) Bragg reflection and gave a first qualitative insight of tilt distribution and strain field, respectively. In the present study, analyses of the (004) and (113) Bragg reflection positions in full 3-dimensional (3D) reciprocal space were performed. A 2D real space area is mapped to render a complete quantitative description of the local lattice tilt, strain, and composition fluctuation of $Si_{0.3}Ge_{0.7}$ films on a step graded buffer.

2. EXPERIMENTAL SETUP

Epitaxial chemical vapor deposition of the SiGe VS was performed on a 300 mm Si(001) wafer using an ASM-Epsilon 3200 reactor. The process gases were dichlorosilane ($SiCl_2H_2$) and germanium tetrachloride ($GeCl_4$) in a high temperature process.[20] To avoid bowing of the wafer by lattice and thermal mismatch with respect to the Si substrate, a BSS of constant $Si_{1-x}Ge_x$ concentration was deposited prior to the VS growth on the frontside of the wafer.[7] The graded $Si_{1-x}Ge_x$ buffer layer on the wafer frontside consists of a graded buffer layer and a constant composition layer on top of the graded part. The total thickness of the graded buffer is 4.9 μm, and the Ge concentration is increased from zero at the interface with the Si(001) substrate to 70% Ge content at the interface with the constant composition layer with an average grading rate of about 15% Ge/μm. The high grade rate is required to keep the total thickness of the buffer layer low. The constant composition $Si_{0.3}Ge_{0.7}$ layer of the as-grown unpolished sample is 1.6 μm thick, which is the focus of our investigations. A nominally identical sample was processed by CMP removing the topmost 600 nm. As a result of the high deposition temperature of the epi process, all parts of the SiGe buffer layer are almost fully relaxed.[20] Figure 1a provides the schematic of the layer stacking. Differential interference contrast (DIC) microscopy images of a selected 90 μm × 90 μm area of the two samples show the characteristic cross-hatch pattern on the ⟨110⟩-equivalent directions of the as-grown sample (Figure 1b), which is clearly absent on the polished surface of the CMP-processed wafer (Figure 1c). The surrounding square frame (visible at the edges of Figure 1b and c) was carved by a focused ion beam (FIB) to define the analyzed region and to ensure that different characterization techniques render results coming from the same region of the sample. The sample morphology was investigated by atomic force microscopy (AFM) using a Nanoscope IV microscope from Digital Instruments operated in tapping mode. The sample was rotated by 45° to better image the cross-hatch within the frame. The new Scanning X-ray Diffraction Microscopy (SXDM) technique K-Map, recently developed at beamline ID01 at the European Synchrotron Radiation Facility (ESRF), was applied to directly image the structural parameters of the $Si_{0.3}Ge_{0.7}$ layer on a micrometer scale (Figure 1d).[16] Here, X-rays

DOI: 10.1021/am508968b
ACS Appl. Mater. Interfaces 2015, 7, 9031−9037

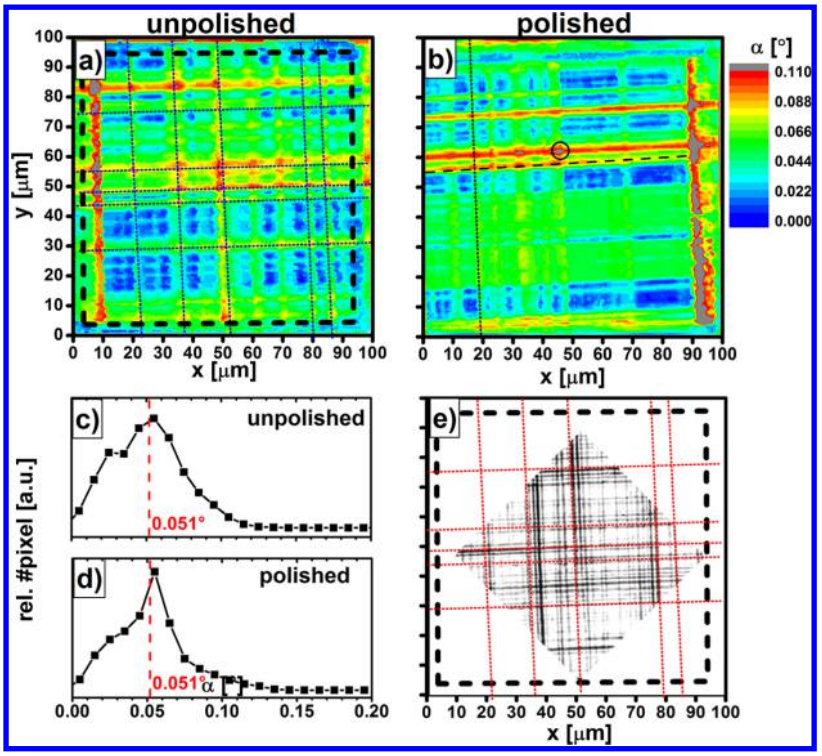

Figure 2. Tilt mappings of the (a) unpolished and (b) polished sample with x and y parallel to ⟨110⟩ directions. Tilt statistics are presented (c) for the unpolished and (d) for the polished samples. (e) Images of the surface gradient resulting from AFM morphology studies of the unpolished sample (see text for details).

with 8 keV were focused by a Fresnel zone plate (FZP) with a beam stop (BS) and an order sorting aperture (OSA) to the center of rotation of the goniometer. A lateral resolution of about 1 μm × 2 μm is achieved in real space. Accordingly, an *x*-*y* piezo stage was used to scan with 750 nm step size the sample area of 100 μm × 100 μm defined by the outer region of the FIB-carved frame (Figure 1b,c). In reciprocal space, the resolution is limited by the beam divergence (<0.05°) and the pixel size (~0.006°). A detailed description of the experimental setup is given in the Supporting Information. The main objective of these investigations was to locally resolve the homogeneity of the top buffer layer with a constant composition of $Si_{0.3}Ge_{0.7}$, namely, to quantify the magnitude of local lattice tilt and strain as well as composition fluctuations on the micrometer scale. For corroboration, spatial averaging laboratory-based high-resolution X-ray diffraction was performed by a Rigaku SmartLab diffractometer making use of SiGe(004) and (224) reflections. Moreover, to investigate the strain distribution in the top SiGe layer region, micro-Raman measurements were carried out using an InVia Renishaw spectrometer in backscattering geometry excited by a 633 nm HeNe laser. An ×100 objective with a numerical aperture of 0.85 was used (focus size of ~0.6 μm), and a region of 80 μm × 80 μm was investigated (step size of 1 μm). Each scan was calibrated using the Ge−Ge mode energy of a Ge(001) bulk crystal reference. It is noted that the Raman penetration depth into the SiGe layer was about 45 nm, while K-Map probes the whole $Si_{0.3}Ge_{0.7}$ layer thickness.

3. RESULTS AND DISCUSSION

3.1. Lattice Tilt. In Figure 2, we report the absolute tilt α map of as-grown and CMP-polished $Si_{0.3}Ge_{0.7}$ layers, respectively (see Supporting Information). Qualitatively, it was found that the spatial variation of the lattice tilt imaging clearly reflects a cross-hatch pattern, whose lines are parallel to the ⟨110⟩ in-plane directions. In general, lines with high tilt values (red-yellow) come up with a low lateral period and lines with low tilts (yellow-green) with higher lateral period. The lines having a higher lateral frequency appear with a tilt around ~0.050° (dotted line in Figure 2b), while less frequent lines feature a higher tilt of around ~0.090° (dashed line in Figure 2b). Furthermore, less than 1% of all analyzed positions have a tilt above 0.110° (gray area). We point out that higher tilt values are in general observed at the intersections of tilt lines. The tilt value at these intersections depends on the amplitude of the contributing tilt lines (see circle in Figure 2b). The tilt values are negligible in between the lines. The plots in Figure 2c and d show the statistical distribution of the tilt values observed within the measured areas for the unpolished and polished samples, respectively. The average tilt of the unpolished as well as polished sample amounts to ~0.051°. Further K-map measurements (see Supporting Information) on similar samples agree with these findings. From additional laboratory-based XRD ω-scans (not shown), resulting from spatially averaged scattering processes, it arises that the measured half-width at half-maximum (HWHM) for the unpolished (0.043°) and polished (0.051°) sample is in the range of the average tilt obtained from the K-map, thus validating these K-map imaging measurements. The main results of the lattice tilt analysis are that (i) tilt images measured by the K-map technique can resolve a cross-hatch pattern in a quantitative way and that (ii) we do not find any quantitative or even qualitative difference between polished and unpolished samples, although they feature very different surface morphologies.

The tilt might be primarily caused by two reasons, namely, by the surface undulation that allows a partial elastic relaxation and/or by the dislocation displacement that causes plastic relaxation. The fact that the polished (without surface undulation contributions) and the unpolished (with surface undulation contributions) samples reflect an identical magnitude of lattice tilt points to dislocations as the main origin of the observed lattice tilt. To strengthen this hypothesis, we

DOI: 10.1021/am508968b
ACS Appl. Mater. Interfaces 2015, 7, 9031−9037

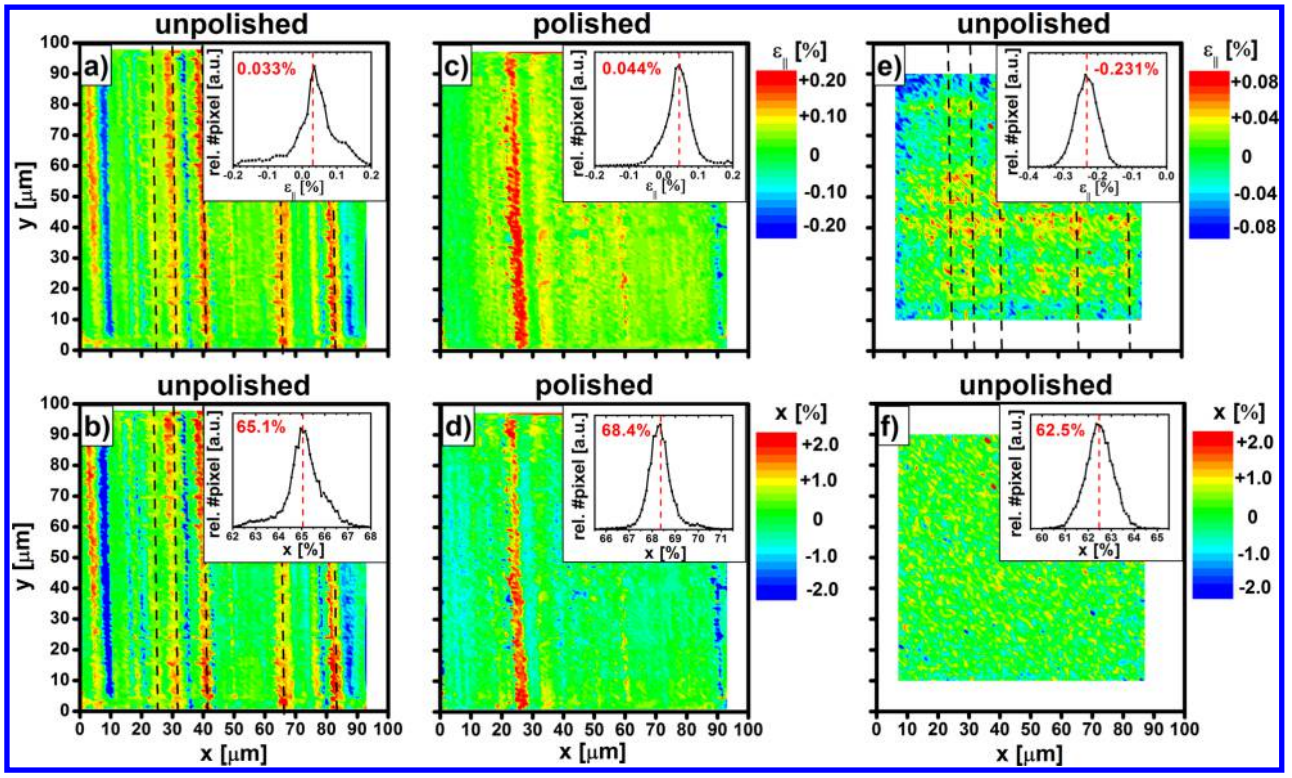

Figure 3. Lateral distribution of strain in the (a) unpolished and (c) polished sample, and composition mapping in the (b) unpolished and (d) polished sample. The respective statistics are given in the insets of the figures. Raman microscopy mappings of (e) strain and (f) composition for the unpolished sample.

correlated the surface morphology with the tilt mapping for the unpolished sample to unveil the contributions from elastic relaxations to the observed lattice tilt images. Figure 2e illustrates the gradient of the surface resulting from the AFM morphology. The positioning of the image was performed according to the FIB frame indicated by the dashed frame in Figures 2a and e. Here, black lines represent higher slope of the surface undulation. Red dotted lines are introduced to guide the eye along selected tilt lines, which can be found in the tilt mapping in Figure 2a. Although the lattice tilt cross-hatch pattern from Figure 2a can be qualitatively identified in the AFM gradient image Figure 2e, it is obvious that not every AFM gradient line can be found in the XRD tilt mapping and vice versa. Thus, no one-to-one correlation can be defined between surface morphology and lattice tilt. This might be related to two reasons: first, the higher spatial resolution of AFM (gradient line distance ∼1 μm) compared to that of the K-Map technique (tilt line distance ∼5 μm) since the X-ray beam projection has to be taken into account. Second, the bulk properties of the $Si_{0.3}Ge_{0.7}$ layer as probed by the K-Map technique are not necessarily manifested in the surface morphology measured by AFM. We thus conclude that, upon comparing the lattice tilt images of polished and unpolished samples, we succeeded to directly quantify the lattice tilt induced by dislocation strain fields with, if any, only minor contributions from the surface undulation.

It is noted that, according to Mooney et al.,[17] these tilt lines are associated with mosaic broadening of the diffraction profile as a result of lattice plane bending due to misfit dislocations.[14,21,22] This nonuniform tilt distribution can be only observed when the tilt regions are similar or even bigger than the footprint of the micro X-ray beam, which occurs when the SiGe film is grown under low mismatch conditions (as in the present case of VSs on a step graded buffer), and thus, sufficiently widely separated, inhomogeneously distributed nucleation sites exist for the dislocation. Thus, a higher observed local tilt might be related to a higher density of 60° dislocations with the same Burger's vector on nearby (111) gliding planes (due to the accumulating screw components), which is the case for sample areas with dislocation pile-ups by, e.g., multiplication mechanisms.[23,24]

3.2. Strain and Composition. The reciprocal space around the (113) reflection was mapped across the same sample area as for the (004) reflection to simultaneously determine strain and composition fluctuations of the topmost $Si_{0.3}Ge_{0.7}$ layer (Figure 3a–d). As a consequnece, strain and composition have been correlated and calculated at each *x*-*y* real space position (see Supporting Information). Qualitatively, no cross-hatch patterns are observed as in the case of the tilt mapping. However, intense lines along the *y*-direction can be identified reflecting the strain and composition fluctuation of the $Si_{0.3}Ge_{0.7}$ layer. Mondiali et al.[19] attributed this observation to the selective sensitivity of the studied (113) reflection to the strain field caused by misfits running only along the in-plane $[1\bar{1}0]$ direction (which is parallel to the *y*-direction in our frame of reference).

Quantitatively, an average value of $\varepsilon_{\parallel}$ = 0.033% with a fwhm of 0.07% is obtained for the in-plane lattice strain of the unpolished sample (Figure 3a). The polished sample shows similar results with $\varepsilon_{\parallel}$ = 0.044% and a fwhm of 0.06% (Figure 3c). An overall tensile strain is observed, which can be explained by the mismatch in the coefficient of thermal expansion (CTE) between SiGe (larger) and pure Si (smaller).[25] Thus, a change from compressive strain to tensile

DOI: 10.1021/am508968b
ACS Appl. Mater. Interfaces 2015, 7, 9031−9037

strain occurs in the SiGe layer during cooling down by accumulating thermal strain.

The analysis of the unpolished sample composition mapping (Figure 3b) shows an average Ge concentration of 65.1% with a fwhm of 1.1%. The polished sample (Figure 3d) has a higher average composition (68.4%) and lower fwhm (0.8%), with a symmetric distribution. This may result from a Ge concentration gradient across the whole 300 mm wafer with lower x toward the edges, as previously observed by Kozlowski et al.[20] on similar samples. The quite homogeneous distribution of the strain and composition was also observed during previous measurements for the unpolished as well as polished samples (see Supporting Information). Additionally, it is noted that these results on the overall magnitude of strain and composition are again corroborated by laboratory-based XRD analysis of the (004) and (224) Bragg reflection (not shown) on a spatially averaged scale.

In conclusion, the strain and composition variation show a homogeneous distribution over the sampled area. It is noted again that no difference can be detected between the unpolished and polished samples. Although such a strain fluctuation was already demonstrated by Raman investigations,[20,26] we are not aware of any study clearly demonstrating the correlation of strain and composition modulation. It is clearly established by the K-map technique that less compressively strained regions at growth temperature (more tensile strained at room temperature) are characterized by a higher germanium concentration. This is indicated as an example for the unpolished case by the black dashed lines in Figure 3a (strain map) and b (composition map) to guide the eyes. This fact points to a decoration mechanism, namely, that germanium with its bigger atomic radius prefers to bind in lattice positions with lower compressive strain, offering thus a larger in-plane lattice constant during growth.

In addition, to corroborate the K-map results, the lateral composition and strain distribution was determined by Raman microscopy in the same sample area. Since the vibration modes of the Ge−Ge, Ge−Si, and Si−Si bonding and, respectively, their signals ω_{GG}, ω_{GS}, and ω_{SS} shift according to stoichiometry and strain, it is possible to determine these values by experimentally approximated equations.[20,27,28] Because of the high germanium concentration, the corresponding Ge−Ge and Ge−Si vibrations give the highest signal intensities and enable the best data evaluation. Thus, ω_{GG} and ω_{GS} peaks were used to map $\varepsilon_{\parallel}$ and x for the unpolished sample in Figure 3e and f, respectively. In the strain mapping (Figure 3e), one can identify a cross-hatch pattern with regions featuring higher tensile strain located at the same positions as determined by K-Mapping (Figure 3a), as indicated by dashed lines. Moreover, the fluctuation is well reflected by the fwhm of the strain (0.07%) and composition (1.2%) distribution. However, in the composition mapping (Figure 3f) no cross-hatch pattern at all can be observed, which is in agreement with previous Raman studies from other authors.[20,26] Furthermore, the absolute values of the average strain ($\varepsilon_{\parallel}$ = −0.23%) and the average composition (x = 62.5%) do not match exactly the XRD results ($\varepsilon_{\parallel}$ = 0.033% and x = 65.1%). Besides the different information depth probed by XRD and Raman, another reason is given by the fact that Raman results are model dependent and thus strongly rely on the accuracy of theoretically and experimentally derived parameters.[28] In particular, the cubic equation for ω_{GS} lacks in precision since the respective Raman frequency value ω^0 for the relaxed alloy is extrapolated due to missing experimental values for $x \rightarrow 0$ (Si rich samples). In contrast, the uncertainties of the elastic constant dependent parameters b_{Si}, b_{SiGe}, and b_{Ge} have a negligible influence at such low strain values. Furthermore, ω_{SS} with its highest sensitivity for the compositional variation has the lowest signal intensity in germanium rich samples (but ω_{GG} and ω_{GS} show only a weak dependence on stoichiometry).[29,30] In contrast, the K-Map technique is based on directly measuring the bulk lattice parameters and orientation, enabling thus a precise, model-free analysis of strain and composition, including even additional information like lattice tilt.

4. SUMMARY AND OUTLOOK

In conclusion, the locally resolved nondestructive K-Map study of the (004) and (113) Bragg reflections enabled us to determine in a correlated way the lattice structure (tilt and strain) as well as the composition of unpolished and polished $Si_{0.3}Ge_{0.7}$ layers with a resolution of about ∼1 μm × 2 μm. K-Map imaging shows reproducible results whose averaged values are in good agreement to classical spatially averaged laboratory-based XRD analysis for tilt, strain, and composition variation (Table 1). Three key results were obtained using the combined techniques: first, the quantified tilt mappings of the $Si_{0.3}Ge_{0.7}$ layer succeed to image the well-known cross-hatch pattern. The XRD derived tilt distribution of the unpolished sample does not necessarily correlate with the AFM derived surface morphology; furthermore, the polished sample does not show any significant difference as compared to the unpolished one with respect to its lattice tilt characteristics. Consequently, the tilt induced by surface undulation does not seem to have noticeable influence on the lattice tilt, as inferred by the lack of qualitative and quantified correlation with the AFM surface gradient distribution. Thus, the comparison of tilt imaging for unpolished and polished samples allows us to quantify the tilt brought about by lattice plane bending due to dislocation strain fields generated by the nonuniform plastic relaxation process.[17] This is an important quantitative result as an input to theory to simulate SiGe VS characteristics.

Table 1. Comparison of Composition and Strain Statistics from K-Map and Laboratory-Based XRD ((004) and (224)) Analysis

	unpolished		polished	
	K-Map	Lab-XRD	K-Map	Lab-XRD
tilt	0.051°	0.043°	0.051°	0.051°
composition	65.1%	65.9%	68.4%	68.8%
strain	0.033%	0.039%	0.044%	0.084%

Second, the correlation between local distribution of strain and composition of the $Si_{0.3}Ge_{0.7}$ layer has been analyzed. The films are under tensile strain on average. This can be explained by the larger CTE of the SiGe film and the over relaxation process from compressive to tensile strain during sample cooling.[27] Moreover, a spatial correlation of the strain with the composition fluctuation was clearly shown. This observation indicates that the composition fluctuation is likely to be driven by the inhomogeneous strain field, resulting in the preferred incorporation of Ge in more relaxed regions on the surface.

Third, no difference in either the tilt, strain, or composition variation could be identified between the unpolished and polished sample. This explains the well-known "memory effect",

DOI: 10.1021/am508968b
ACS Appl. Mater. Interfaces 2015, 7, 9031−9037

which leads to a rather fast reappearance of a cross-hatch pattern during regrowth after a CMP process.

Finally, the advanced K-Map imaging technique has been shown to be a model free, nondestructive, and quantitative method for extracting key structural parameters including local strain, film composition fluctuations, and lattice tilt variations from $Si_{1-x}Ge_x$ films. The innovative K-map technique provides valuable input to device engineers for evaluating the variations of sub-20 nm CMOS technologies that cannot be achieved with any other technique. It provides a realistic picture of the materials homogeneity of SiGe VS prepared on 300 mm wafers.

Certainly, a number of interesting future K-map experiments can be easily envisioned to study either the in situ growth process or in-operando characteristics of semiconductor heterostructures. In terms of growth optimization, the high attenuation length of X-rays will enable one, by the choice of the corresponding Bragg peaks, to study buried layer structures and thus monitor the relaxation process of each layer structure of an advanced semiconductor heterostructure in a locally resolved way. Where in-operando studies are concerned, electrical contact layers of advanced semiconductor diode heterostructures can, for example, be investigated with respect to thermal load effects under electrical stress, thus enabling in future important materials science insights on, e.g., drift and degradation mechanisms of semiconductor heterostructure devices.

■ ASSOCIATED CONTENT

Supporting Information

Details of the experimental setup; information about the real space and reciprocal space resolution; underlying calculations of the tilt, strain, and composition are explained; local congruence of the (004) and (113) Bragg reflection is supported by plotting the local q_x and q_y values; investigations of local tilt, strain, and composition from previous measurements on similar samples, corroborating the reliability of the results and the K-map technique. This material is available free of charge via the Internet at http://pubs.acs.org.

■ AUTHOR INFORMATION

Corresponding Author

*Tel: +49 335 5625 637. Fax: +49 335 5625 681. E-mail: zoellner@ihp-microelectronics.com.

Notes

The authors declare no competing financial interest.

■ REFERENCES

(1) Del Alamo, J. A. Nanometre-Scale Electronics with III–V Compound Semiconductors. *Nature* **2011**, *479*, 317–323.

(2) Takagi, S.; Kim, S. H.; Yokoyama, M.; Zhang, R.; Taoka, N.; Urabe, Y.; Yasuda, T.; Yamada, H.; Ichikawa, O.; Fukuhara, N.; Hata, M.; Takenaka, M. High Mobility CMOS Technologies Using III–V/Ge Channels on Si Platform. *Solid-State Electron.* **2013**, *88*, 2–8.

(3) Paul, D. J. Si/SiGe Heterostructures: From Material and Physics to Devices and Circuits. *Semicond. Sci. Technol.* **2004**, *19*, R75–R108.

(4) Moontragoon, P.; Soref, R. A.; Ikonic, Z. The Direct and Indirect Bandgaps of Unstrained $Si_xGe_{1-x-y}Sn_y$ and Their Photonic Device Applications. *J. Appl. Phys.* **2012**, *112*, 073106.

(5) Wirths, S.; Geiger, R.; von den Driesch, N.; Mussler, G.; Stoica, T.; Mantl, S.; Ikonic, Z.; Luysberg, M.; Chiussi, S.; Hartmann, J. M.; Sigg, H.; Faist, J.; Buca, D.; Grützmacher, D. Lasing in Direct-Bandgap GeSn Alloy Grown on Si. *Nat. Photonics* **2015**, *9*, 88–92.

(6) Fitzgerald, E. A.; Xie, Y. H.; Green, M. L.; Brasen, D.; Kortan, A. R.; Michel, J.; Mii, Y. J.; Weir, B. E. Totally Relaxed Ge_xSi_{1-x} Layers with Low Threading Dislocation Densities Grown on Si Substrates. *Appl. Phys. Lett.* **1991**, *59*, 811–813.

(7) Storck, P.; Vorderwestner, M. Semiconductor Wafer with a Heteroepitaxial Layer and a Method for Producing the Wafer. US20090236695A1, Sep 24, 2009.

(8) Currie, M. T.; Samavedam, S. B.; Langdo, T. A.; Leitz, C. W.; Fitzgerald, E. A. Controlling Threading Dislocation Densities in Ge on Si Using Graded SiGe Layers and Chemical-Mechanical Polishing. *Appl. Phys. Lett.* **1998**, *72*, 1718–1720.

(9) Kishinu, S.; Ogirima, M.; Kurata, K. A Cross-Hatch Pattern in $GaAs_{1-x}P_x$ Epitaxially Grown on GaAs Substrate. *J. Electrochem. Soc.* **1972**, *119*, 617–622.

(10) Hsu, J. W. P.; Fitzgerald, E. A.; Xie, Y. H.; Silverman, P. J.; Cardillo, M. J. Surface Morphology of Related Ge_xSi_{1-x} Films. *Appl. Phys. Lett.* **1992**, *61*, 1293–1295.

(11) Albrecht, M.; Chistiansen, S.; Michler, J.; Dorsch, W.; Strunk, H. P. Surface Ripples, Crosshatch Pattern, and Dislocation Formation: Cooperating Mechanisms in Lattice Mismatch Relaxation. *Appl. Phys. Lett.* **1995**, *67*, 1232–1234.

(12) Fitzgerald, E. A.; Xie, Y. H.; Monroe, D.; Silverman, P. J.; Kuo, J. M.; Kortan, A. R.; Thiel, F. A.; Weir, B. E. Relaxed Ge_xSi_{1-x} Structures for III-V Integration with Si and High Mobility Two-Dimensional Electron Gases in Si. *J. Vac. Sci. Technol., B* **1992**, *10*, 1807–1819.

(13) Tersoff, J. Dislocations and Strain Relief in Compositionally Graded Layers. *Appl. Phys. Lett.* **1993**, *62*, 693–695.

(14) Holy, V.; Li, J. H.; Bauer, G.; Schäffler, F.; Herzog, H. J. Diffuse X-ray Scattering from Misfit Dislocations in SiGe Epitaxial Layers with Graded Ge Content. *J. Appl. Phys.* **1995**, *78*, 5013–5021.

(15) Benediktovitch, A.; Ulyanenkov, A.; Rinaldi, F.; Saito, K.; Kaganer, V. M. Concentration and Relaxation Depth Profiles of $In_xGa_{1-x}As$/GaAs and $GaAs_{1-x}P_x$/GaAs Graded Epitaxial Films Studied by X-ray Diffraction. *Phys. Rev. B* **2011**, *84*, 035302.

(16) Chahine, G. A.; Richard, M.-I.; Homs-Regojo, R. A.; Tran-Caliste, T. N.; Carbone, D.; Jacques, V. L. R.; Grifone, R.; Boesecke, P.; Katzer, J.; Costina, I.; Djazouli, H.; Schroeder, T.; Schülli, T. Imaging of Strain and Lattice Orientation by Quick Scanning X-ray Microscopy Combined with Three-Dimensional Reciprocal Space Mapping. *J. Appl. Crystallogr.* **2014**, *47*, 762–769.

(17) Mooney, P. M.; Jordan-Sweet, J. L.; Noyan, I. C.; Wang, P. C.; Kaldor, S. K. Observation of Local Tilted Regions in Strain-Relaxed SiGe/Si Buffer Layers Using X-ray Microdiffraction. *Appl. Phys. Lett.* **1999**, *74*, 726–728.

(18) Mochizuki, S.; Sakai, A.; Taoka, N.; Nakatsuka, O.; Takeda, S.; Kimura, S.; Ogawa, M.; Zaima, S. Local Strain in SiGe/Si Heterostructures Analyzed by X-ray Microdiffraction. *Thin Solid Films* **2006**, *508*, 128–131.

(19) Mondiali, V.; Bollani, M.; Cecchi, S.; Richard, M.-I.; Schülli, T.; Chahine, G.; Chrastina, D. Dislocation Engineering in SiGe on Periodic and Aperiodic Si(001) Templates Studied by Fast Scanning X-ray Nanodiffraction. *Appl. Phys. Lett.* **2014**, *104*, 021918.

(20) Kozlowski, G.; Fursenko, O.; Zaumseil, P.; Schroeder, T.; Vorderwestner, M.; Storck, P. The Epitaxial Growth of Low Defect SiGe Buffer Layers for Integration of New Materials on 300 mm Silicon Wafers. *ECS Trans.* **2012**, *50*, 613–621.

(21) Mooney, P. M. Strain Relaxation and Dislocations in SiGe/Si Structures. *Mater. Sci. Eng.* **1996**, *R17*, 105–146.

(22) Mooney, P. M.; LeGoues, F. K.; Chu, J. O.; Nelson, S.F. F.K. Nucleation of Dislocations in SiGe Layers Grown on (001)Si. *Appl. Phys. Lett.* **1993**, *62*, 3464–3977.

(23) LeGoues, F. K.; Meyerson, B. S.; Morar, J. F.; Kirchner, P. D. Mechanism and Conditions for Anomalous Strain Relaxation in Graded Thin Films and Superlattices. *J. Appl. Phys.* **1992**, *71*, 4230–4243.

(24) Samavedam, S. B.; Fitzgerald, E. A. Novel Dislocation Structure and Surface Morphology Effects in Relaxed Ge/Si-Ge(Graded)/Si Structures. *J. Appl. Phys.* **1997**, *81*, 3108–3116.

(25) Capellini, G.; de Seta, M.; Zaumseil, P.; Kozlowski, G.; Schroeder, T. High Temperature X-ray Diffraction Measurements on

DOI: 10.1021/am508968b
ACS Appl. Mater. Interfaces 2015, 7, 9031–9037

Ge/Si(001) Heterostructures: A Study on the Residual Tensile Strain. *J. Appl. Phys.* **2012**, *111*, 073518.
(26) Chen, H.; Li, Y. K.; Peng, C. S.; Liu, H. F.; Huang, Q.; Zhou, J. M. Crosshatching on a SiGe Film Grown on a Si(001) Substrate Studied by Raman Mapping and Atomic Force Microscopy. *Phys. Rev. B* **2002**, *65*, 233303.
(27) Capellini, G.; de Seta, M.; Busby, Y.; Pea, M.; Evangelisti, F.; Nicotra, G.; Spinella, C.; Nardone, M.; Ferrari, C. Strain Relaxation in High Ge Content SiGe Layers Deposited on Si. *J. Appl. Phys.* **2010**, *107*, 063504.
(28) Perova, T. S.; Wasyluk, J.; Lyutovich, K.; Kasper, E.; Oehem, M.; Rode, K.; Waldron, A. Composition and Strain in Thin $Si_{1-x}Ge_x$ Virtual Substrates Measured by Micro-Raman Spectroscopy and X-ray Diffraction. *J. Appl. Phys.* **2011**, *109*, 033502.
(29) Pezzoli, F.; Grilli, E.; Guzzi, M.; Sanguinetti, S.; Chrastina, D.; Isella, G.; von Känel, H.; Wintersberger, E.; Stangl, J.; Bauer, G. Strain-Induced Shift of Phonon Modes in $Si_{1-x}Ge_x$ Alloys. *Mater. Sci. Semicond. Process.* **2006**, *9*, 541−545.
(30) Pezzoli, F.; Sanguinetti, S.; Bonera, E.; Grilli, E.; Guzzi, M. Modelling of the Phonon Strain Shift Coefficients in $Si_{1-x}Ge_x$ Alloys. *J. Phys.: Conf. Ser.* **2007**, *92*, 012152.
(31) Kriegner, D.; Wintersberger, E.; Stangl, J. Xrayutilities: A Versatile Tool for Reciprocal Space Conversion of Scattering Data Recorded with Linear and Area Detectors. *J. Appl. Crystallogr.* **2013**, *46*, 1162−1170.
(32) Zaumseil, P.; Kozlowski, G.; Schubert, M. A.; Yamamoto, Y.; Bauer, J.; Schülli, T. U.; Tillack, B.; Schroeder, T. The Role of SiGe Buffer in Growth and Relaxation of Ge on Free-Standing Si(001) Nano-Pillars. *Nanotechnology* **2012**, *23*, 355706.
(33) Wortman, J. J.; Evans, R. A. Young's Modulus, Shear Modulus, and Poisson's Ratio in Silicon and Germanium. *J. Appl. Phys.* **1965**, *36*, 153−156.
(34) Dismukes, J. P.; Ekstrom, L.; Pfaff, R. J. Lattice Parameter and Density in Germanium-Silicon Alloys. *J. Phys. Chem.* **1964**, *68*, 3021−3027.

DOI: 10.1021/am508968b
ACS Appl. Mater. Interfaces 2015, 7, 9031−9037